Water Resources Research

RESEARCH ARTICLE
10.1029/2019WR026686

Flow Resistance and Energy Dissipation in Supercritical Air-Water Flows Down Vegetated Chutes

B. Scheres[1], **H. Schüttrumpf**[1], **and S. Felder**[2]

[1]Institute of Hydraulic Engineering and Water Resources Management, RWTH Aachen University, Aachen, Germany, [2]Water Research Laboratory, School of Civil and Environmental Engineering, UNSW Sydney, NSW 2052, Australia

Key Points:
- Unique study of flows down vegetated chutes highlighted the effects of vegetation upon flow patterns, flow aeration, and flow resistance
- Measurements with phase-detection intrusive probes provided direct estimates of aeration, flow resistance, and energy dissipation
- Air-water flow properties must be considered in the design of supercritical flows down vegetated chutes

Supporting Information:
- Supporting Information S1
- Movie S1
- Movie S2
- Movie S3
- Movie S4
- Movie S5
- Movie S6

Correspondence to:
B. Scheres,
scheres@iww.rwth-aachen.de

Citation:
Scheres, B., Schüttrumpf, H., & Felder, S. (2020). Flow Resistance and Energy Dissipation in Supercritical Air-Water Flows Down Vegetated Chutes. *Water Resources Research*, *56*, e2019WR026686. https://doi.org/10.1029/2019WR026686

Received 1 JUL 2019
Accepted 1 FEB 2020
Accepted article online 6 FEB 2020

Abstract Vegetation covers on dikes and embankment dams have proven as sustainable and cost-effective surface protection against external erosion caused by hydraulic, mechanical, or climatic impacts. Determination of the hydraulic loads that act upon these covers requires the knowledge of the flow resistance. While the high-velocity flows on vegetated slopes are often aerated, the flow aeration has rarely been considered, and no direct measurements of the air-water flow properties have been conducted to date. The air-water flow properties are needed for a direct estimation of important design parameters such as friction factors and residual head at the downstream end. Herein, unique air-water flow measurements were conducted in high-velocity air-water flows down a vegetated chute with a 1:3 slope. Several vegetation covers were tested for a range of flow rates. The experiments revealed strong flow aeration within three-dimensional, fragmented flows associated with complex interactions of vegetation and high-velocity flows. The air-water flow properties were measured with phase-detection intrusive probes providing novel insights into aerated flows on vegetated chutes including distributions of void fraction, bubble count rate, and interfacial velocity as well as direct estimates of energy dissipation and flow resistance. The results highlighted strong flow aeration and energy dissipation for all vegetated configurations. The median equivalent Darcy-Weisbach friction factors for all vegetations were within 0.19 to 0.45, comparable to aerated flows on stepped spillways. The present results highlighted the significant flow resistance of vegetated covers and the need to consider air-water flow properties in the design of vegetated chutes.

1. Introduction

Natural and nature-based solutions in the water resources field have drawn attention due to opportunities of, for example, increasing biodiversity, provision of habitats, regulating services, such as carbon sequestration or water purification, and the offer of cultural services. In terms of coastal and flood protection, flow or wave attenuation and sediment retention are valuable ecosystem services of coastal and riverine ecosystems (Barbier et al., 2011; Gutiérrez et al., 2011). New insights into the hydraulic efficiency and cost efficiency of natural and nature-based solutions pave the way for integration of such solutions into engineering design processes (de Vriend et al., 2015; Morris et al., 2018; Narayan et al., 2016; Schoonees et al., 2019; Sutton-Grier et al., 2018).

Dikes and flow conveyance structures are traditionally built as firm artificial structures having important functions for flood protection and mitigation. For structural stability of dikes, an erosion-resistant dike cover is necessary to withstand hydraulic loads from steady overflows (river dikes) or unsteady wave overtopping (sea dikes). Dams require a sufficient flood release structure to dissipate the flow's energy in case of a flood event. The ecological value of dikes and embankment dams can be enhanced with a vegetation cover that provides surface protection for moderate hydraulic loads. The vegetation is often a composition of grass species that create a closed sward providing sufficient erosion resistance (CIRIA, 2013).

Typically, the design of vegetated covers is based upon the anticipated hydraulic loads (design parameters) and the maximum tolerable loads (limiting values). For sea dikes, the limiting values are described by maximum tolerable wave overtopping discharges (EurOtop, 2018) and for river dikes and embankment dams by a combination of flow velocity and loading duration during steady overflows (CIRIA, 2013; Hewlett et al., 1987). Imperfections, such as bare spots, mice holes, or mole burrows, represent weak spots with lower hydraulic resistance (EurOtop, 2018; Le et al., 2017). The design parameters are determined by empirical

equations that describe the flow parameters during overflow and overtopping (Dean et al., 2010; Schüttrumpf & Oumeraci, 2005). These empirical equations are based upon hydraulic boundary conditions, such as water levels and wave heights, as well as chute parameters, such as channel slope or bed roughness. One parameter is the flow resistance, which is often expressed in terms of the Darcy-Weisbach friction factor f. For the landward slope of a grass-covered dike, Hughes (2011) estimates $0.04 \leq f \leq 0.08$. However, the friction factors for vegetated chutes are not fully explored yet (Hughes, 2011), leading to uncertainties in the hydraulic design of vegetated chutes.

The effects of vegetation on flow velocity, turbulence, and flow resistance in nonaerated flows have been studied extensively (Mossa et al., 2017; Murphy et al., 2007; Nepf, 2012a; J. Q. Yang et al., 2015). Generally, the flows can be distinguished into flows with submerged or unsubmerged vegetation as hydraulic processes and flow resistance are largely influenced by the ratio of vegetation height to water depth (e.g., Nepf, 2012b). Herein, submerged or unsubmerged vegetation processes are similar to submerged or unsubmerged roughness elements (e.g., Bathurst, 1988; Best, 2002).

Unsubmerged flows are defined as flow cases in which the deflected vegetation height exceeds the water depth and plants protrude through the flow. In these cases, the friction factor f is typically calculated using the Darcy-Weisbach equation (e.g., Chanson, 2004) approximating the energy gradient by the surface slope (Abrahams et al., 1994; Pan et al., 2016; Zhao et al., 2016). Studies of overland flows with shallow flow depths and unsubmerged or barely submerged vegetation revealed a large variability of Darcy-Weisbach friction factors including $0.5 \leq f \leq 18.8$ for laminar flows on a grassland hillslope (Abrahams et al., 1994) and $3.41 \leq f \leq 69.53$ for laminar flows on grass-plot surfaces (Pan et al., 2016). For supercritical, turbulent flows in a channel with artificial unsubmerged vegetation stems, Zhao et al. (2016) observed $0.47 \leq f \leq 1.12$. In studies which considered the vegetation resistance as the dominant mechanism, flow resistance was expressed in terms of a drag coefficient (Chapman et al., 2015; Kothyari et al., 2009).

In flows with submerged vegetation, the deflected vegetation height is smaller than the water depth, and the friction factor is typically calculated using the Darcy-Weisbach equation (Järvelä, 2002; Velasco et al., 2003). Friction factors for submerged vegetation were reported in open channel flow studies, mostly focusing on subcritical flows. For a submerged grass surface, Järvelä (2002) estimates $0.18 \leq f \leq 1.93$. Velasco et al. (2003) observed $0.1 \leq f \leq 1.57$ for submerged artificial river plants in flume experiments. In both studies, the friction factors decreased with increasing Reynolds numbers (Järvelä, 2002; Velasco et al., 2003). While subcritical open channel flows have been studied extensively, the flow resistance in supercritical, vegetated flows has been rarely studied (Kothyari et al., 2009).

Overflow or overtopping of dikes or embankments leads to highly turbulent, supercritical flows which are often strongly aerated, leading to flow bulking and effecting the flow resistance (Chanson, 1994; Scholl, 2016). Measurements of the flow depths without consideration of the entrained air lead to an overestimation of the actual clear water depth affecting the quantification of flow resistance and energy dissipation (e.g., Cantré et al., 2017). If free-surface flows are aerated, the flow aeration must be considered, but to the authors' knowledge, no previous study has considered the air-water flow properties in the estimation of the flow resistance and energy dissipation capacities of vegetated surfaces in supercritical, aerated flows. Therefore, the friction factors from previous flow resistance studies may not be directly applicable to supercritical, aerated flows on vegetated chutes.

Extensive research on flow resistance in supercritical, aerated flows has been conducted in nonvegetated hydraulic conveyance structures with typical embankment dam slopes, such as smooth spillways (Anderson, 1965; Cain & Wood, 1981; Felder & Severi, 2016; Straub & Anderson, 1960; Wood, 1983), stepped spillways (e.g., Felder & Chanson, 2015c; Hunt et al., 2014), gabion stepped spillways (Wüthrich & Chanson, 2014), and rock chutes (Pagliara et al., 2010). These and many further studies used phase-detection intrusive probes to measure the air-water flow properties and to estimate the design parameters including flow resistance and energy dissipation performance. Typical equivalent Darcy-Weisbach friction factors for such aerated flows are $0.008 \leq f_e \leq 0.061$ for very smooth chutes (Severi, 2018), $0.1 \leq f_e \leq 0.4$ for stepped spillways (Felder & Chanson, 2015c), and $0.41 \leq f_e \leq 4.59$ for rock chutes (Pagliara et al., 2010). The commonly applied air-water flow measurement and data processing methods can be directly applied to vegetated chutes. Herein, unique measurements of air-water flow properties were conducted on several full-scale vegetated chutes with a 1:3 slope ($\theta = 18.4°$) and submerged vegetation. Similar to previous studies on the flow

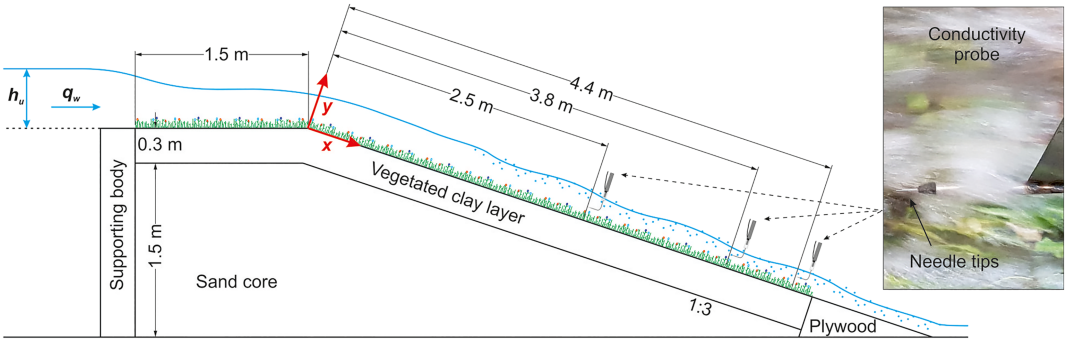

Figure 1. Sketch of the experimental setup including dimensions; photo of double-tip conductivity probe and locations of air-water flow measurements.

resistance of vegetation (e.g., Cantré et al., 2017; Järvelä, 2002), the flow resistance analyses were based on the Darcy-Weisbach equation, but taking into account flow aeration. The results provided novel insights into flow aeration, energy dissipation performances, and flow resistance in high-velocity supercritical flows down vegetated chutes with submerged vegetation.

2. Experimental Setup and Configurations

2.1. Facility and Instrumentation

Experiments were conducted in a 20-m long, 2-m wide, and up to 3-m high spillway facility at the Institute for Hydraulic Engineering and Water Resources Management (IWW) of RWTH Aachen University. A 1:3 sloped chute with a range of vegetation covers was constructed within the facility comprising a sand core built against an impermeable stone-filled gabion wall sealed with a coated plywood plate (Figure 1). A partition wall centered along the chute divided the chute into two test sections of approximately 1-m width, and two different test configurations were installed in parallel. A sealing element at the upstream end of the chute allowed for separate testing of each test section.

Steady and calm inflows into the test section were supplied via a 1.5-m long broad-crested weir from a large upstream reservoir with a surface area of 21 m^2. Water was supplied from a header tank providing steady inflows into the upstream reservoir. After passing the test section, water entered an underground water storage and was pumped into the header tank in a closed water circuit. The flow rates were controlled via the water level upstream of the broad-crested weir h_u using the weir equation with discharge coefficients specifically determined for the various test configurations based on the conductivity probe measurements. The discharge coefficient obtained for the nonvegetated chute was consistent with standard values for broad-crested weirs (e.g., Press & Schröder, 1966). Lower discharge coefficients were found for the vegetated chutes as a result of increased roughness due to the vegetation. Further information on the determination of the overflow discharges and discharge coefficients are given in the supporting information. Although a less permeable, clayey soil (see section 2.2) was used as vegetation subsoil, small infiltration and consequently some loss of flow during the overflow process cannot be ruled out. The investigated flow conditions are given in Table 1 including the discharge per unit width q_w, the Reynolds number defined in terms of the hydraulic diameter $Re = 4q_w/\upsilon$, where υ is the kinematic viscosity of water, the mean flow velocity $u_w = q_w/\left(\int_0^{Y_{90}} (1-C)\cdot dy\right)$, where C is the time-averaged local void fraction and Y_{90} the characteristic flow depth where $C = 0.9$, and the shear stress $\tau = \rho_w \cdot g \cdot S_f \cdot \left(\int_0^{Y_{90}} (1-C)\cdot dy\right)$ as average factor along the chute for $2.5 \le x \le 4.4$ m, where ρ_w is the density of water, g the gravitational acceleration, and $S_f = -\partial H/\partial x$ the friction slope (Henderson, 1966). Additionally, Table 1 provides details on the test configurations including botanical information, that is, the average vegetation height h_{veg} measured with a rising plate meter modified

Table 1
Experimental Configurations Including Details on Vegetations

Reference	Vegetation description	Number of species	Vegetation reinforcement	c_{veg} (%)	h_{veg} (mm)	q_w (m^2/s)	Re (−)	u_w (m/s)	τ (N/m^2)
TV1	Species-poor grass-dominated mixture	4	—	82	51	0.041–0.180	$1.6–7.2 \cdot 10^5$	1.2–3.7	78–218
TV4	Grass-herb mixture	10	—	73	60	0.045–0.102	$1.8–4.1 \cdot 10^5$	1.1–2.5	111–125[a]
TV4grid	Grass-herb mixture	10	Geogrid	68	61	0.045–0.215	$1.8–8.6 \cdot 10^5$	1.1–3.9	119–244[a]
TV5	Species-rich herb-dominated mixture	18	—	88	68	0.040–0.098	$1.6–3.9 \cdot 10^5$	1.1–2.4	91–150[a]
TV5grid	Species-rich herb-dominated mixture	18	Geogrid	60	57	0.029–0.114	$1.2–4.6 \cdot 10^5$	0.9–2.4	76–221
NV	No vegetation. Smooth plywood	—	—	—	—	0.022–0.187	$0.9–7.5 \cdot 10^5$	2.1–5.1	68–91[a]

[a]Average values along the chute for $2.5 \leq x \leq 4.4$ m not available for all tests as measurements were conducted only at two of the three measuring locations for some tests.

from Castle (1976) and the average grade of vegetation coverage c_{veg} estimated with the auxiliary tables of Gehlker (1977). Flow rates were incrementally increased for each configuration; for the two lowest flow rates $q_w \leq 0.045$ m^2/s, experiments were conducted for 45 minutes and for all larger discharges for 30 minutes. The onset of critical erosion processes of the chute cover, that is, erosion reaching the sand core (generally only as model effects at the channel walls), provided the upper limit of tested flow conditions for each of the vegetated configurations (Table 1).

To determine the flow resistance along the vegetated chutes, air-water flow measurements were performed at three locations using three double-tip conductivity probes from UNSW Water Research Laboratory (WRL) (Figure 1). Each probe consisted of two identical needle tips, which were separated in streamwise direction by $x = 4.82$, 4.88, and 5.80 mm, respectively, and by $z \approx 1$ mm in transverse direction. Each probe tip consisted of a needle tip with a platinum wire of 0.125 mm as the inner electrode and an outer stainless-steel electrode of 0.6 mm. Both electrodes were insulated by epoxide, resulting in a sudden drop in resistivity if the needle tip was in air, corresponding to a raw voltage of about 0.5 V and to a voltage of about 4.3 V when the probe tip was in water. The WRL double-tip conductivity probes have been previously successfully benchmarked against other phase-detection probes in high-velocity air-water flows (Felder et al., 2019; Felder & Pfister, 2017), and further details on the working principles can be found in Cartellier (1990), Chanson (2002a), and Felder and Pfister (2017). The conductivity probes were carefully placed in flow direction perpendicularly to the chute to optimize the piercing of the air-water interfaces with the needle tips. A small patch of vegetation was cut just upstream of the probe tips of the conductivity probes to avoid adverse effects of the vegetation on the air-water flow measurements and to minimize potential impact of the vegetation on the probes. The probes were vertically shifted for a profiling of the air-water flow properties. The probes' raw signals were sampled at 20 kHz for 20 s using a WRL LabVIEW acquisition software and the multifunction data acquisition device NI USB-6002. Although a longer sampling time would be preferable (Felder & Chanson, 2015b), the sampling time in the present experiments was reduced to minimize erosion processes of the vegetation.

The raw voltage signals of the conductivity probes were postprocessed with the air-water data analysis software of Felder (2018) comprising a single threshold analysis with 50% of the bimodal peak of the probability distributions of the raw voltage signals at each measurement location and a cross-correlation analysis of the two simultaneously sampled leading and trailing tip signals. The single-threshold analysis provided the time-averaged local void fraction C and the number of changes of air-water interfaces, that is, the bubble count rate F. The maximum cross-correlation coefficients for the two probe signals provided the average travel time between the two probe tips and the local time-averaged interfacial velocity V. Further details on the data processing can be found in Chanson (2002a) and Felder (2013). All raw data was checked for potential adverse effects of vegetation on the probes' leading and trailing tips to remove potential suspicious results from the analysis. When vegetation impacted

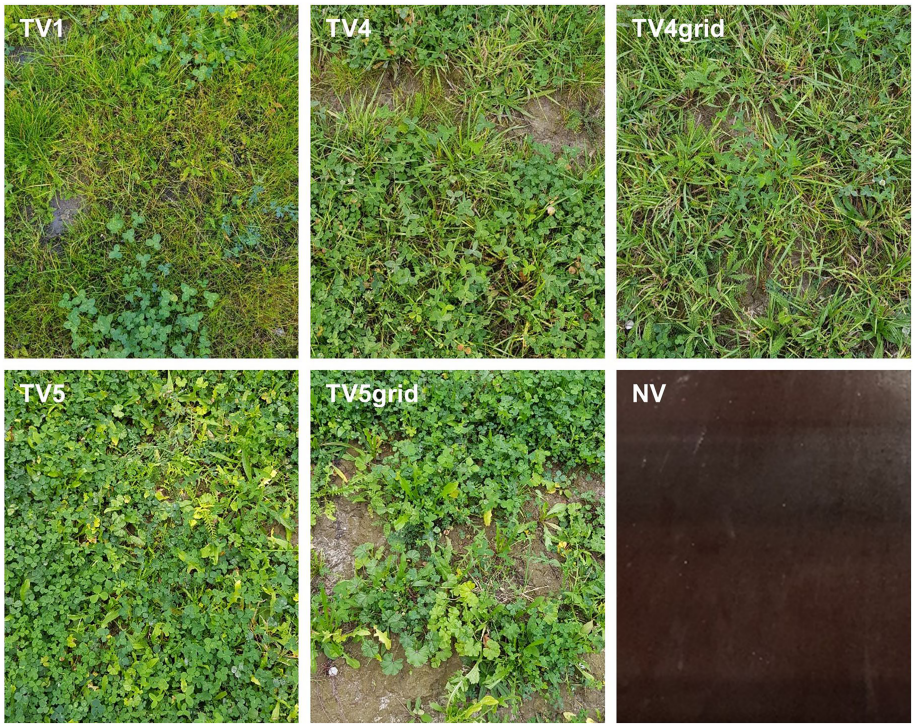

Figure 2. Illustration of vegetation covers highlighting the type of vegetation and the vegetation coverage as well as a smooth configuration for comparison.

upon the probe tips, three cases were observed including suspicious signals of either leading or trailing tip for the whole sampling time, for a short period during the sampling time or a change in signal strength for part of the sampling time. A typical raw voltage signal of the conductivity probes and examples of suspicious signals are given in the supporting information. In cases where the leading tip was affected, the data at that measurement location were not considered. When suspicious data were observed only for the trailing tip, the void fraction and bubble count rates of the leading tip were considered but the interfacial velocities were excluded. Adverse effects of vegetation on any of the probe tips were found for less than 4% of the measurements.

2.2. Experimental Configurations

Several vegetated chute covers were tested (Table 1; Figure 2). The composition of the vegetation combined optimized ecological value under consideration of the erosion resistance (Graunke & Wrage-Mönnig, 2018; Scheres et al., 2018). Vegetation TV1 represented a species-poor grass-dominated vegetation mixture, which is commonly applied on German sea dikes (EAK, 2002). TV1 served as reference vegetation. Further vegetation compositions were a grass-herb mixture (TV4) and species-rich herb-dominated mixture (TV5). Two vegetation configurations were reinforced with the soil reinforcement grid Fortrac® 3D by HUESKER, which is a flexible, three-dimensional geogrid of 10-mm thickness with an average weight of 550 g/m^2 made from high-tensile PET with a polymer coating (Table 1).

All vegetations were cultivated in planter trays in the courtyard of IWW. As substrate, a clay with approximately 10% of the material having grain diameters <0.002 mm and 10% >0.063 mm and a median grain size diameter d_{50} = 0.009 mm determined from sieve and sedimentation analysis was used. During the vegetation period of around 6 months (April–October 2018), regular maintenance and documentation of the vegetation was conducted (Scheres et al., 2018). Figure 2 illustrates the vegetations prior to testing. Table 1 provides further details on the vegetation configurations including botanical information. Due to exceptional weather conditions during the vegetation period with heavy rains at the beginning and a long heat wave in summer, the vegetation had some bare patches. For

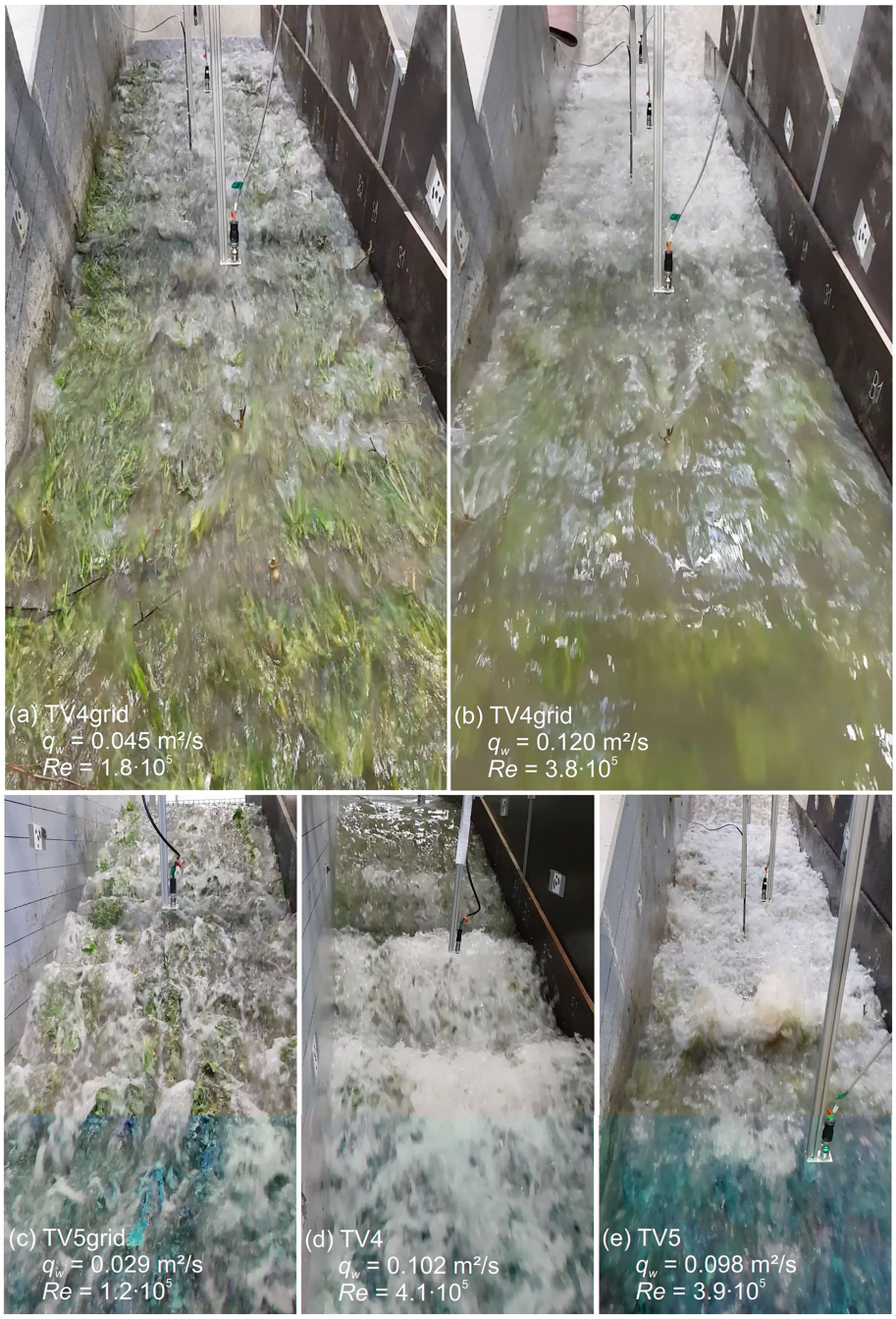

Figure 3. Photos of air-water flow patterns along the vegetated chutes. (a), (b), and (e) view in flow direction; (c) and (d) view against flow direction.

consistency, the experiments with all vegetations were conducted within a time frame of less than 3 weeks. The vegetations were grown in segments of 0.3-m thick clay elements with 1.5-m length and 1.0-m width, which were lifted into the experimental test section. The vegetated configurations were complemented with a nonvegetated chute (NV) made of smooth plywood. All configurations were installed along the full length of the chute including the broad-crested weir at the upstream end. Further photos of the different test configurations are provided in the supporting information.

3. Flow Patterns on the Vegetated Chutes

Figure 3 shows photos of typical air-water flow patterns on the vegetated chutes. These visual impressions are supported by short video clips and additional photographic material in the supporting information.

For all test configurations, the flows were unaerated at the upstream end of the chute. Along the chute, the flow patterns varied depending upon the test configuration and flow conditions. Apart from the nonvegetated chute (see Movie S6), all vegetated configurations experienced strong flow aeration along the chute (see Movies S1–S5). For all vegetated configurations, three-dimensional flow features and irregular aeration patterns were observed, which were directly linked to the vegetation characteristics. General vegetation characteristics, such as the elasticity, as well as local differences in vegetation structure, for example, bare spots or scattered more rigid vegetation that acted as flow barrier, influenced the flow. The vegetation in configuration TV1 was easily bent by the flow creating an almost uniform vegetation layer with few local differences in surface patterns. The flow patterns were comparatively smooth with almost no aeration observed along the upper part of the chute and steady aeration downstream of the inception point of free-surface aeration (see Movie S1). For all other vegetation configurations, the vegetations had consistently more rigid stems or larger leaves that had a strong influence on the flow patterns including increased overall aeration as well as increased three-dimensionality of the flows, leading to strong local flow aeration (see Movies S2–S5). In addition to vegetation types and elasticity, surface irregularities in the form of bare spots influenced the flow patterns, leading to local jet formation with flow aeration downstream of bare spots when the high-velocity flow impacted upon vegetation.

For small discharges, $q_w \leq 0.045$ m^2/s, fragmented flows with local aeration along the whole length of the chute occurred for all vegetated configurations (Figure 3a). Main parts of the vegetation were already submerged, even for the lowest discharges. Single taller or more rigid plants, however, still represented obstacles where flow was deflected. Local aeration was mainly induced around vegetation irregularities including bare spots or rigid vegetation, leading to variable local flow aeration along the chute (Figure 3a). Irrespective of the vegetated configuration, the flow aeration increased overall along the chute based on visual observations (Figure 3a). Local flow deflections were observed around higher or more rigid vegetation (Figure 3c). The configuration TV1 had only little local aeration within the upper part of the chute due to the even and elastic vegetative cover, whereas the other vegetated configurations showed more local aeration due to a higher number of bare patches or more rigid vegetation.

While the flows were three-dimensional for small discharges, they became more uniform with increasing flow rate. The overall flow depth increased, fully submerging the vegetation and shifting the inception point of free-surface aeration downstream. The flows were mainly unaerated along the upper part of the chute. At some distance downstream, an onset of aeration was observed at the inception point of free-surface aeration, that is, the location where the turbulent fluctuations close to the free-surface were large enough to overcome surface tension (Figure 3b). For large flow rates, local aeration upstream of the inception point of free-surface aeration was only observed in very few cases, for example, during tests with configuration TV4grid, which had a single wooden, rigid plant on the upper part of the chute which deflected and aerated the flows locally even for higher discharges (Figure 3b).

In addition to local aeration features, such as shown in Figure 3e indicating increased aeration and flow bulking downstream of a bare spot when the high-velocity flow impacted upon vegetation, some bed features extended across the full width of the channel. For example, most probably as a consequence of cross-sectional bare stripes at the beginning of testing, pronounced stepped aeration patterns were formed for configuration TV4 (Figure 3d). In this case, aeration occurred across the full width of the chute, leading to a fixation of the inception point of free-surface aeration at this location for most flow rates. For configurations TV1, TV4grid, and TV5grid, the location of the inception point of free-surface aeration shifted downstream with increasing discharges in agreement with previous research on spillways, for example, Felder and Chanson (2013).

The tests with the smooth configurations were significantly different, showing no flow aeration for any flow conditions. While the high-velocity flows were fully developed, the bed roughness and the chute slope were

insufficient to initiate flow aeration (see Movie S6). The flows were characterized by free-surface roughness as observed for similarly sloped smooth chutes (Felder & Severi, 2016). With increasing flow rate, the inception point of free-surface roughness migrated downstream.

4. Air-Water Flow Properties

This section presents typical distributions of air-water flow properties. All air-water flow data are provided in the supporting information. The air-water flow properties confirmed the significance of the flow aeration on the vegetated chutes, highlighting the need to incorporate flow aeration in the estimation of the rate of energy dissipation and the flow resistance.

The dimensionless distributions of void fraction are shown for all tests in Figure 4 as a function of the dimensionless flow depth y/Y_{90}. All void fraction profiles showed typical S-shapes, although differences were observed depending upon the vegetation, the flow condition, and the measurement location. Higher data scatter was noticed for low void fractions, probably as a result of vegetation influencing aeration in the lower water column as well as potential vegetation submergence of the probe tips. Void fraction profiles for configuration TV1 were similar for all flow conditions with little differences between measurement positions. Larger differences were found for the other vegetated configurations, especially TV5 and TV5grid, which showed irregular variations in C distributions at the three measuring positions indicating changing aeration patterns along the chute. In some cases, a downward shift of the void fraction distributions with increasing flow rate was noticed, indicating an increase of aeration along the water column with increasing flow rate. Data scatter reflected the complexity of the flows over vegetated chutes as well as local hydraulic effects due to vegetation cover and type or bare spots. These hydraulic effects varied depending upon the reaction of the vegetation to increasing flow rates altering the local void fraction distributions. For the smooth chute, only free-surface roughness without actual air entrainment occurred, which resulted in steeper C-profiles for the smooth chute compared to the C-profiles of the vegetated chutes. The void fraction distributions were compared with the advective diffusion equation for air bubbles on smooth invert spillways by Toombes and Chanson (2007):

$$C = 1 - \tanh^2\left(K' - \frac{\frac{y}{Y_{90}}}{2D'}\right), \tag{1}$$

where K' is a dimensionless integration constant

$$K' = 0.327 + \frac{1}{2D'}, \tag{2}$$

and D' is a dimensionless diffusivity

$$C_{mean} = 2D'\left(\tanh\left(K'\right) - 0.316\right), \tag{3}$$

where C_{mean} is the depth-averaged void fraction

$$C_{mean} = \frac{1}{Y_{90}} \int_0^{Y_{90}} C \cdot dy. \tag{4}$$

Figure 4 shows the advective diffusion equation for selected flow conditions for all configurations. Despite data scatter and the vegetation effects on local aeration, the present data agreed overall well with the advective diffusion equation for smooth invert spillways (Figure 4).

The range of C_{mean} for the vegetated chutes ($0.14 \leq C_{mean} \leq 0.41$ with an average value of $C_{mean} \approx 0.25$) compared well with observations of aerated flows on rock chutes of $0.20 \leq C_{mean} \leq 0.37$ for $14.8° \leq \theta \leq 20.8°$ (Pagliara et al., 2010) and stepped chutes of $0.15 \leq C_{mean} \leq 0.46$ for $3.4° \leq \theta \leq 26.6°$ (Felder & Chanson, 2015a). The close agreement with previous studies on fully aerated spillway flows confirmed the significance of flow aeration in supercritical flows down vegetated slopes. C_{mean} for the smooth chute was lower than for the vegetated chutes and scattered around $C_{mean} = 0.11$ on average.

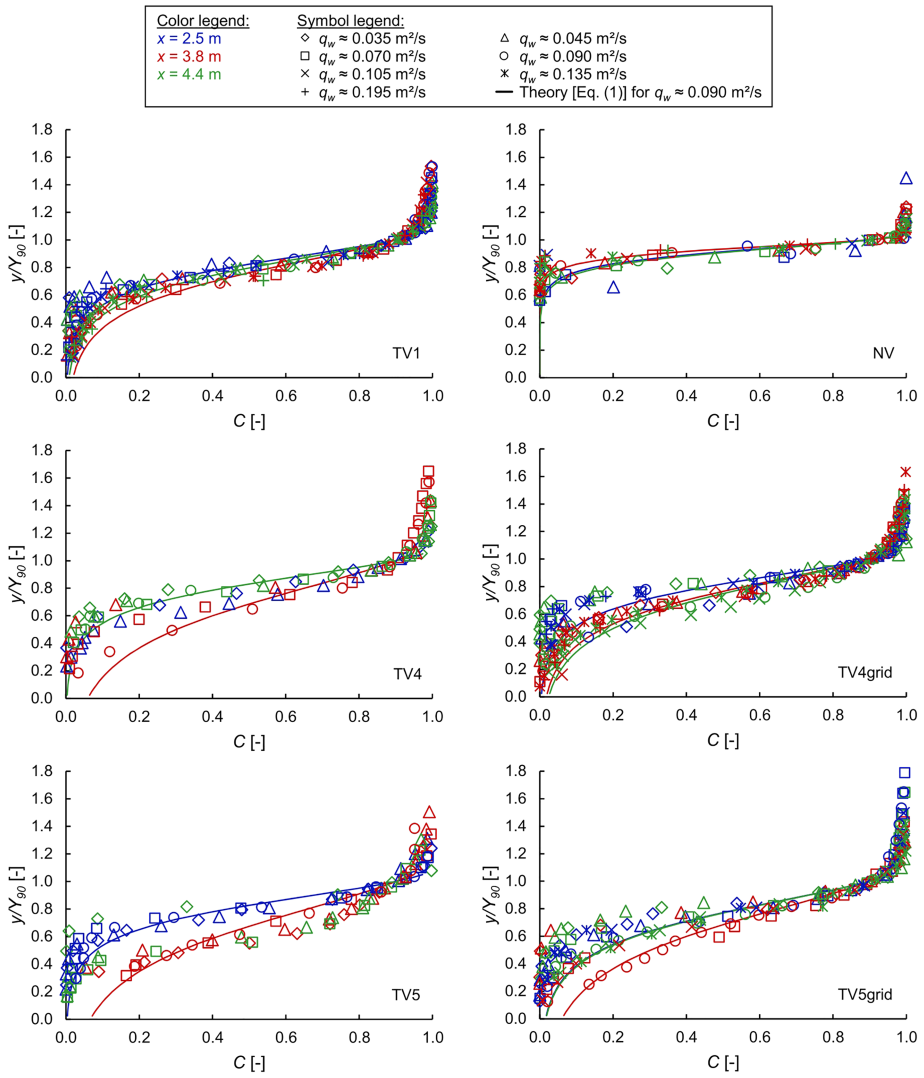

Figure 4. Distributions of void fraction C on vegetated and smooth chutes with $\theta = 18.4°$ as function of the dimensionless flow depth y/Y_{90} for all tested discharges q_w; x giving the longitudinal distance along the slope; TV1 = species-poor grass-dominated mixture, TV4 = grass-herb mixture, TV5 = species-rich herb-dominated mixture, NV = smooth slope, grid = geogrid reinforcement; comparison of experimental data with the advective diffusion equation for air-water flows on smooth invert spillways of Toombes and Chanson (2007) (equation (1)).

Figure 5 shows the distributions of the dimensionless interfacial velocity V/V_{90} for each test configuration as function of y/Y_{90}. While configuration TV1 had very similar velocity distributions for all flow conditions, all other vegetated configurations showed much stronger data scatter. The interfacial velocities were influenced by local irregularities of the vegetation structure, such as rigid vegetation or bare spots that led to local flow effects, which were also discharge related. The interfacial velocity distributions were compared with a power law for $y/Y_{90} \leq 1$ (equation (5)) and a uniform profile for $y/Y_{90} > 1$.

$$\frac{V}{V_{90}} = \left(\frac{y}{Y_{90}}\right)^{\frac{1}{N}} \text{ for } \frac{y}{Y_{90}} \leq 1, \tag{5}$$

where V_{90} is the characteristic interfacial velocity where $C = 0.9$ and N is the power law exponent. The power law exponent was determined for each configuration resulting in $2.6 \leq N \leq 3.7$ (with $0.61 \leq R^2 \leq 0.76$). The parameters for each vegetated configuration are shown in Figure 5. Similar trends were found for all vegetated chutes. On average, a power law exponent of 3.0 was achieved for the vegetated chutes, valid for

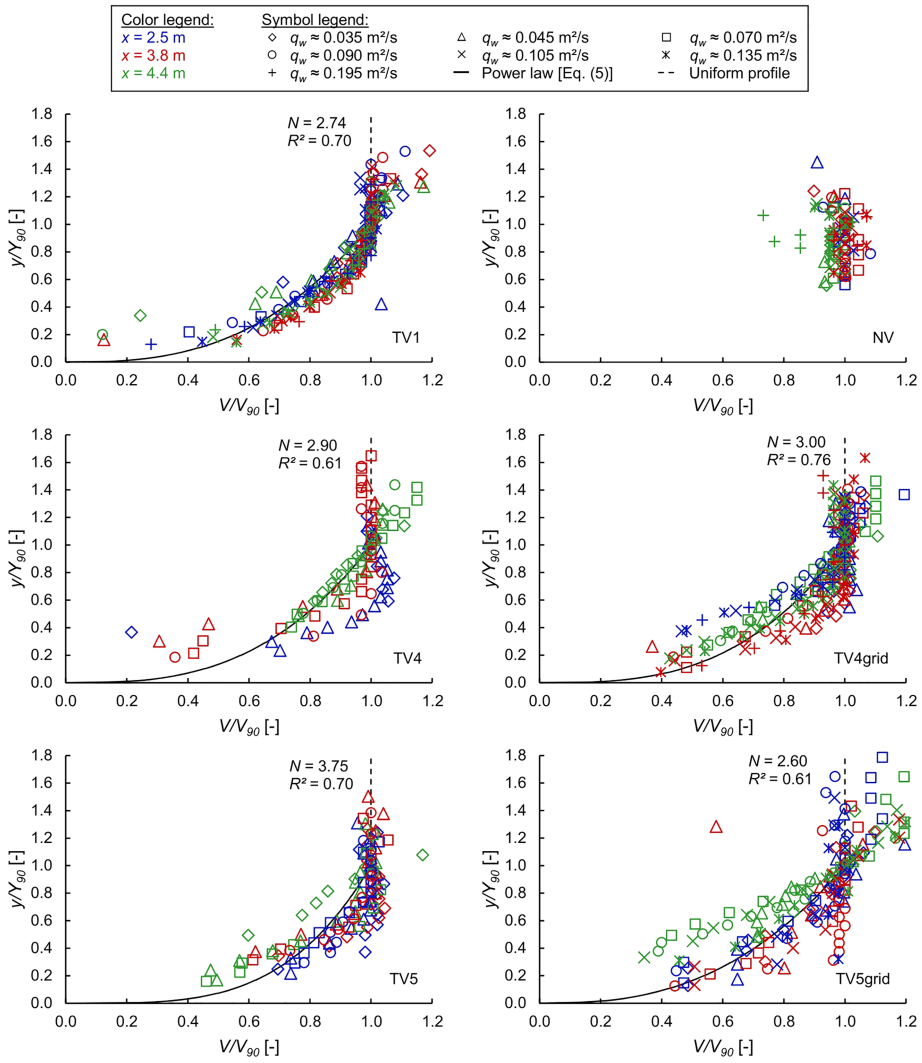

Figure 5. Distributions of dimensionless interfacial velocity V/V_{90} on vegetated and smooth chutes with $\theta = 18.4°$ as function of the dimensionless flow depth y/Y_{90} for all tested discharges q_w; x giving the longitudinal distance along the slope; TV1 = species-poor grass-dominated mixture, TV4 = grass-herb mixture, TV5 = species-rich herb-dominated mixture, NV = smooth slope, grid = geogrid reinforcement; comparison of experimental data with power law (equation (5)) and uniform profile.

approximately $0.2 \leq y/Y_{90} \leq 1$. Below $y/Y_{90} = 0.2$, the effects of the vegetation are likely to yield a very different profile (see, e.g., Nepf, 2012a). No resemblance of the present velocity profiles to the S-shaped velocity distributions observed in rockfill channel flows (Bathurst, 1988; Ferro & Baiamonte, 1994) was found. The power law exponents of the present study are smaller than the power law exponents from studies on stepped chutes with $N = 6$ (Hunt et al., 2014) and $N = 10$ (Felder & Chanson, 2015c), or $N = 4.5$ (Severi, 2018) for smooth chutes at laboratory scale and $N = 6.3$ for the full-scale smooth chute data of Cain and Wood (1981). The present power law exponents were similar to $N = 3.5$, which was reported in supercritical flows across macro-roughness elements downstream of a sluice gate (Felder & Chanson, 2016). The smaller power law exponents are linked to influences of the vegetation that caused lower velocities close to the channel bed. Even smaller power law exponents were found for rockfill channel flows with $N \approx 1$ (Chanson, 2002b based on Bathurst, 1988 and Ferro & Baiamonte, 1994), illustrating the strong influence of the bed structure on the velocity distribution. Flow studies with submerged vegetation often use the logarithmic law of the wall above the vegetated layer and a uniform layer within the vegetation, or a mixing layer scheme with two constant velocities above and

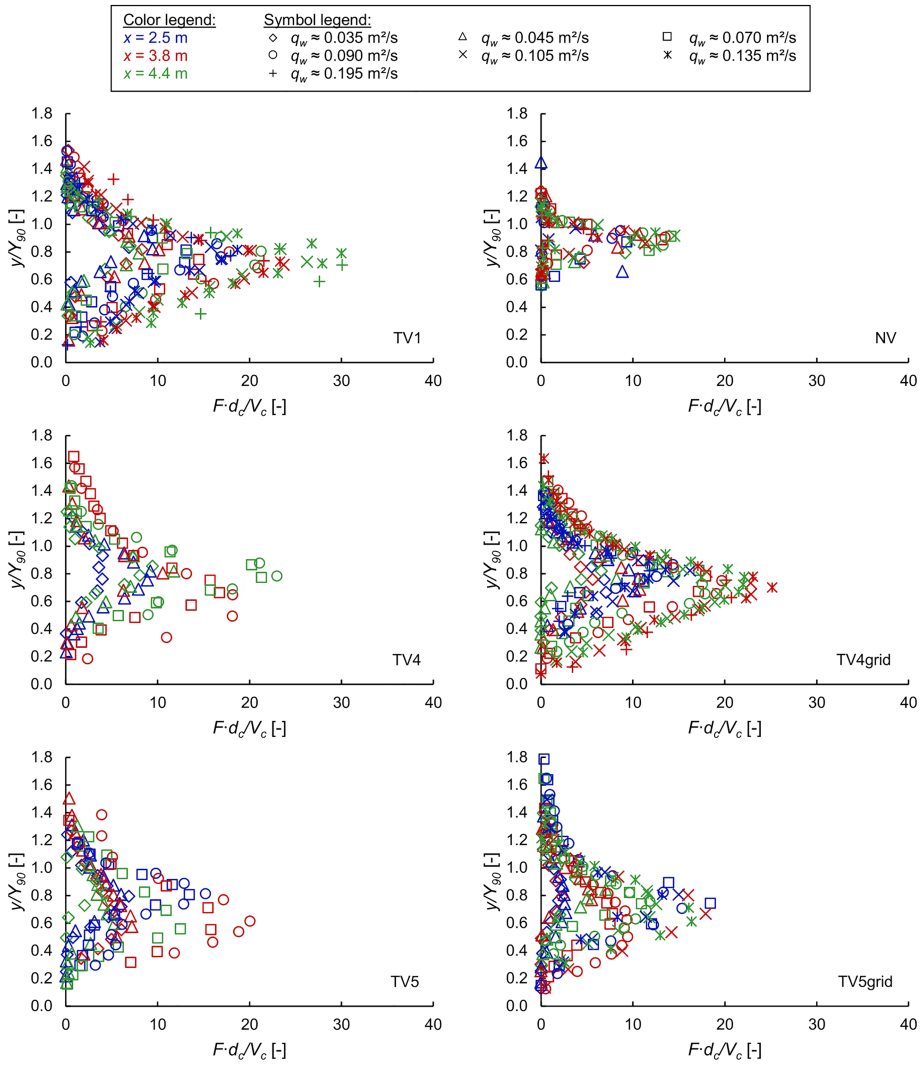

Figure 6. Distributions of dimensionless bubble count rate $F \cdot d_c/V_c$ on vegetated and smooth chutes with $\theta = 18.4°$ as function of the dimensionless flow depth y/Y_{90} for all tested discharges q_w; x giving the longitudinal distance along the slope; TV1 = species-poor grass-dominated mixture, TV4 = grass-herb mixture, TV5 = species-rich herb-dominated mixture, NV = smooth slope, grid = geogrid reinforcement.

within the vegetation to describe their velocity profiles (Gambi et al., 1990; Lightbody & Nepf, 2006; Nepf, 2012b; Termini, 2015; W. Yang & Choi, 2010). To apply such approaches to the present configurations, a more detailed description of the vegetation morphology, for example, the deflected vegetation height, is needed.

Figure 6 shows the distributions of the dimensionless bubble count rate $F \cdot d_c/V_c$ for each test configuration, where d_c and V_c are the critical depth and velocity, respectively. Large bubble count rates were observed for all vegetated configurations with a distinct maximum in bubble count rate F_{max} for a flow depth $y/Y_{90} \approx 0.75$ (total range: $0.50 \leq y/Y_{90} \leq 0.93$) and $C \approx 0.48$ (total range: $0.27 \leq C \leq 0.78$). The largest bubble count rate was observed for configuration TV1 at the downstream end of the chute with $F_{max} = 266$ Hz. Close to the channel bed and close to the free-surface $y/Y_{90} > 1.2$, F tended to zero. In general, F increased with increasing flow rate, which is in agreement with previous studies of high-velocity air-water flows (e.g., Chanson & Toombes, 2002; Felder et al., 2019; Zhang & Chanson, 2017).

As the number of measurement positions along the chute was limited to three points, it was not possible to provide details about the longitudinal evolution of the air-water flow parameters. Based upon the available

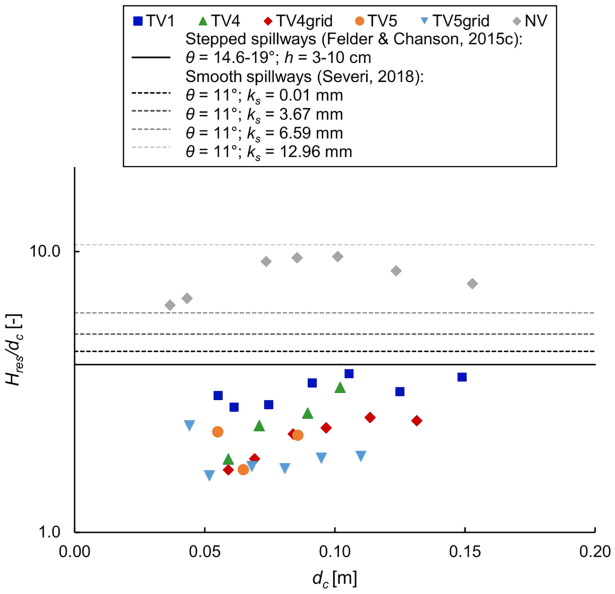

Figure 7. Dimensionless residual energy H_{res}/d_c at the downstream end of vegetated and smooth chutes with $\theta = 18.4°$ as function of the critical flow depth d_c; TV1 = species-poor grass-dominated mixture, TV4 = grass-herb mixture, TV5 = species-rich herb-dominated mixture, NV = smooth slope, grid = geogrid reinforcement; comparison of present data with median values (solid and dashed lines) of previous studies on smooth and stepped chutes where h is the step height and k_s the equivalent sand roughness height.

data and the observations of the flow patterns, the flow conditions appeared to be nonuniform at the downstream end of the chute for all vegetated configurations and for all flow rates.

5. Energy Dissipation and Flow Resistance

5.1. Residual Energy

The residual energy H_{res} at the downstream end of the chute is a key design parameter providing information of the energy dissipation capacity along a chute. For all configurations, the residual energy was calculated at the downstream end of the slope $x = 4.4$ m based on the air-water flow measurements:

$$H_{res} = \int_0^{Y_{90}} (1-C)\cdot\cos\theta\cdot dy + \frac{q_w^2}{2g\cdot\left(\int_0^{Y_{90}} (1-C)\cdot dy\right)^2}. \quad (6)$$

The dimensionless residual energy H_{res}/d_c is shown as a function of the critical flow depth d_c in Figure 7. The median values, standard deviations, and 95% confidence intervals of H_{res}/d_c are summarized in Table 2.

While the median dimensionless residual energies of the various vegetated chutes were within a relatively narrow band $1.77 \leq H_{res}/d_c \leq 3.17$, trends between the different vegetations were identified which were consistent with observations of flow patterns. Configuration TV1 showed smoother flow conditions during the model tests and resulted in the largest residual energies at the downstream end of the chute. Higher elasticity of the vegetation led to early bending of the leaves and stems so that flow interaction was reduced and less energy was dissipated. For configuration TV5grid, in contrast, the lowest residual energies at the downstream end of the chute were found consistent with much more fragmented flow patterns along the vegetated chute. For the same vegetation mixture (vegetated configurations TV5 and TV5grid), a lower vegetation coverage for TV5grid resulted in lower residual energies at the downstream end of the chute. Although bare spots appeared to be favorable in terms of energy dissipation, the disadvantageous effects of weak spots for erosion resistance (EurOtop, 2018; Le et al., 2017) have to be kept in mind if no further protective measures such as reinforcing geogrids are employed. The residual energy for the smooth slope $6.4 \leq H_{res}/d_c \leq 9.6$ was calculated for comparison showing significantly higher residual energy compared to the vegetated configurations (Figure 7).

To highlight the significant energy dissipation capacity for the vegetated chutes, results of air-water flow studies on smooth and stepped spillways with comparable slopes are included in Figure 7. The dimensionless residual energies of the unvegetated chute (NV) are in good agreement with the results of Severi (2018) for smooth spillways despite some data scatter. For stepped spillways with embankment slopes of $14.6° \leq \theta \leq 19°$, Felder and Chanson (2015c) determined a median dimensionless residual energy of $H_{res}/d_c = 3.96$ combining the results of all relevant stepped spillway studies with air-water flow measurements. Felder and Chanson (2015c) mention explicitly that these data corresponded to nonuniform air-water flow conditions at the downstream end of the stepped spillways and that the median value of all available data sets combined with the standard deviation ($H_{res}/d_c = 3.45$ for lower and $H_{res}/d_c = 4.48$ for upper limit) should be used to determine the residual head. The present nonuniform residual head data at the downstream end of the vegetated chutes are therefore directly comparable to the stepped spillway data. The dimensionless residual energies for the vegetated chutes were overall lower compared to the stepped spillway data, highlighting the significant energy dissipation capability of vegetated chutes. The energy dissipation was linked with the surface roughness of the vegetation as well as three-dimensional interactions of the flow with the vegetation.

Table 2
Median Values and Standard Deviation of Dimensionless Residual Energy at the Downstream End of the Chutes and Equivalent Darcy-Weisbach Friction Factors

	TV1	TV4	TV4grid	TV5	TV5grid	NV
Median H_{res}/d_c (−)	3.17	2.53	2.30	2.22	1.77	8.55
Standard deviation (−)	±0.34	±0.61	±0.37	±0.33	±0.28	±1.30
95% confidence interval (−)	±0.25	±0.60	±0.29	±0.38	±0.23	±0.96
Median f_e (−)	0.19	0.44	0.30	0.41	0.45	0.04
Standard deviation (−)	±0.04	±0.01	±0.03	±0.05	±0.15	±0.01
95% confidence interval (−)	±0.03	±0.02	±0.03	±0.05	±0.12	±0.01

5.2. Flow Resistance

The flow resistance was represented by the equivalent Darcy-Weisbach friction factor f_e based upon the air-water flow data at the three measurement locations:

$$f_e = \frac{8 \cdot g \cdot S_f \cdot \left(\int_0^{Y_{90}} (1-C) \cdot dy \right)^3}{q_w^2}. \quad (7)$$

The equivalent friction factors f_e are average factors along the chute for $2.5 \leq x \leq 4.4$ m. All results are presented in Figure 8 as function of $h_{veg} \cdot c_{veg}/D_H$, where D_H is the hydraulic diameter. Corresponding median values, standard deviations, and 95% confidence intervals are summarized in Table 2. Median friction factors for the vegetated chutes were $0.19 \leq f_e \leq 0.45$. The lowest median friction factor was obtained for configuration TV1 and the largest for configuration TV5grid. This finding was consistent with the different vegetation characteristics and the associated interactions of the flows with the vegetation leading to increased energy dissipation. Data scattering within each test configuration was generally low with exception of an outlier for configuration TV5grid for reasons unknown. For small discharges, single taller or more rigid vegetation was not yet fully submerged and acted locally as macro-roughness (see section 3). The friction factors, however, scattered only within a small range, and no significant differences were observed for the tested flow conditions. Thus, no clear effects of local macro-roughness were identified within the present study. For higher vegetation or smaller discharges, effects due to macro-roughness should be considered. The smooth surface (NV) resulted in $f_e = 0.04$ on average, which was well below the friction factors of the vegetated chutes.

Median friction factors of smooth and stepped chutes were included in Figure 8a for comparison. Friction factors of the unvegetated chute (NV) were in good agreement with the results of Severi (2018) for smooth spillways. For stepped chutes, $0.1 \leq f_e \leq 0.4$ was found for typical embankment slopes (Felder & Chanson, 2015c). Friction factors of the vegetated chutes were similar or above the stepped spillway data. The present data were also compared to the median friction factors for rock chutes (Pagliara et al., 2010), indicating slightly smaller friction factors. Like flow processes on stepped and rock chutes, the surface roughness of the vegetation and the interaction of the flow with the vegetation led to high flow resistance.

Figure 8b compares the present vegetation data in supercritical fully aerated flows with friction factors from previous studies on open channel flow with submerged vegetation. The overall range of present friction factors $0.15 \leq f_e \leq 0.82$ was within the wide range of previous open channel flow studies on flow resistance (Järvelä, 2002; Velasco et al., 2003). Note that these studies were performed in subcritical flows.

The relationship between equivalent Darcy-Weisbach friction factors on the vegetated chutes and Reynolds and Froude numbers at the downstream end, respectively, was also investigated (figure in supporting information). While previous studies in subcritical open channel flows with vegetation reported decreasing friction factors with increasing Reynolds numbers (Järvelä, 2002; Velasco et al., 2003), the present aerated supercritical flows on the vegetated chutes did not confirm this trend. Instead, the flow resistance appeared to be more or less independent of the Reynolds number for $1.2 \cdot 10^5 \leq Re \leq 7.2 \cdot 10^5$. The relationship between f_e and the Froude number showed a general trend of decreasing friction factors with increasing Froude number, endorsing the results of Kothyari et al. (2009), who found the same trend in drag force measurements in supercritical flows through vegetation.

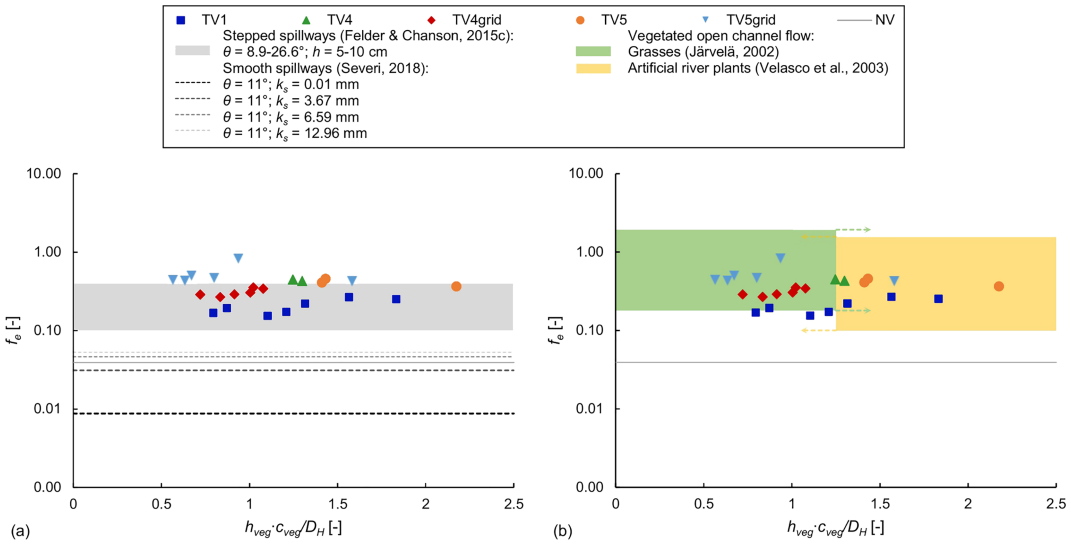

Figure 8. Equivalent Darcy-Weisbach friction factors f_e for vegetated and smooth chutes with $\theta = 18.4°$ as function of $h_{veg} \cdot c_{veg}/D_H$, where h_{veg} is the average vegetation height, c_{veg} the average grade of vegetation coverage and D_H the hydraulic diameter; TV1 = species-poor grass-dominated mixture, TV4 = grass-herb mixture, TV5 = species-rich herb-dominated mixture, NV = smooth slope, grid = geogrid reinforcement; comparison of present data with previous studies on (a) smooth and stepped chutes, where h is the step height and k_s the equivalent sand roughness height, and (b) open channel flow with submerged vegetation; Lines = median values; Shaded areas = range of data; Note that data in (b) from literature on vegetated open channel flow overlap (indicated by arrows).

The present tests were performed with real vegetations that, by nature, were characterized by irregular vegetation cover with bare spots influencing the hydraulic processes in general and locally. Thus, the experiments were subject to inherent uncertainties, even though up-to-date instrumentation (double-tip conductivity probes) and analysis approaches were applied. While the flows were found to be locally fragmented and three-dimensional, the flow motions were dominantly in streamwise direction, enabling the calculation of air-water flow properties of the flow. However, small uncertainties in the measurement of the air-water flow properties along the chute may exist, which may have directly affected the determination of the equivalent Darcy-Weisbach friction factors. Additionally, the estimation of the flow rate is affected by uncertainties in terms of flow velocity and flow depths and potential infiltration, which may have also affected the determination of the equivalent Darcy-Weisbach friction factors. For future investigations of vegetated chutes, it is recommended that the number of air-water flow measurement locations be increased to better account for the three-dimensional flow patterns and flow irregularities.

Flow-induced reconfiguration of vegetation influences the flow resistance until an equilibrium state is reached (Nepf, 2012b). Tests of the present study were performed with grasses and herbs that, from visual observations, showed overall a high elasticity and quickly adjusted to the flow before the measurements were started. Thus, no effects of flow-induced reconfiguration of the vegetation are expected. However, as a result of natural processes, erosion altered the surface of the vegetated chutes, and single plants were ripped out during the tests. For short-term loads (1 hr) and plain grass in average condition, a design velocity of 3.8 m/s is recommended (Hewlett et al., 1987). The vegetated chutes experienced mean flow velocities between 0.9 and 3.9 m/s (see Table 1). Superficial, slowly progressing erosion occurred during all tests, particularly at bare spots. No erosion was observed that would be considered a failure of the dike cover; that is, erosion did not reach the sand core (except due to model effects at the channel walls). The surface conditions of the chute covers after failure at the channel walls are illustrated in the supporting information. Plant losses (mainly clover) were noticed for TV5. The present flow resistance analyses do not consider flow-induced surface alterations and thus give only momentary values. Influences from surface alterations that progressed during the measuring phase cannot be ruled out (general issue of continuous profile measurements) and may induce uncertainties for the flow resistance analysis. The flow-induced reconfiguration and its influence on the flow resistance are an interesting issue for future research. The erosion resistance of the chute covers is not closer described in this manuscript.

6. Conclusions

Full-scale model tests on a smooth and five vegetated chutes with $\theta = 18.4°$ were conducted for a range of stationary discharges $q_w \leq 0.215$ m²/s to investigate the flow aeration and flow resistance of high-velocity aerated flows on vegetated chutes. Nonaerated flows were observed for the smooth chute, while the vegetation led to significant flow aeration due to the increased bed roughness as well as flow fragmentation. Depending on the vegetation, the flow and aeration patterns differed ranging from comparatively smooth aerated flows for a grass-dominated vegetated chute (TV1) to a much rougher flow with irregular aeration at bare spots and rigid vegetation for the sparsely grown herb-dominated chute (TV5grid).

Measurements of the air-water flow properties were conducted with state-of-the-art double-tip conductivity probes at three positions along the chute, providing unique insights into the air-water flow properties in supercritical flows on vegetated chutes. The results showed a strong flow aeration for all vegetated chutes. The flows were overall complex and three-dimensional, and local effects such as jet formations or deflections caused by rigid vegetation or bare spots resulted in some data scatter for the air-water flow properties void fraction, bubble count rate, and interfacial velocities. Despite this data scatter, the results highlighted the significant aeration on the chutes and the need to consider flow aeration in the assessment of flow resistance and erosion processes on vegetated dikes and embankments.

The energy dissipation performance and the flow resistance were calculated based upon the air-water flow data. Large energy dissipation capability was found for the vegetated chutes. For the dense grass-dominated mixture, the residual energies were similar to stepped spillways, while the sparsely grown herb-dominated mixture showed even lower residual energies at the downstream end of the chute. Similar trends were found in terms of the flow resistance. The equivalent Darcy-Weisbach friction factors were similar or exceeded the results of stepped spillways. Median friction factors for the vegetated chutes were within $0.19 \leq f_e \leq 0.45$. The vegetation affected the air-water flows, resulting in significant energy dissipation and flow resistance. Although bare spots seemed to be favorable in terms of energy dissipation and flow resistance, they may lead to a reduced erosion resistance of the chute. Further research is required to optimize the design of vegetated chutes for both flow and erosion resistance.

The present results are only valid for particular vegetations and hydraulic loads. Hydraulic processes, energy dissipation, and flow resistance are most likely to change for other vegetation covers and hydraulic loads. The consistency in results for the present five vegetation covers provides, however, a first guidance on the overall magnitude of flow resistance in vegetated channels under supercritical flow conditions.

Unique measurements of aeration, energy dissipation, and flow resistance in supercritical, aerated flows down vegetated chutes have been conducted. The aeration effects on flow bulking, flow resistance, and energy dissipation were considered using typical two-phase flow instrumentation and data processing methods for high-velocity air-water flows. Herein, the present results provided novel insights into important design parameters of vegetated chutes as well as the need to consider the flow aeration in any future studies of air-water flows on vegetated chutes.

Notation

C	void fraction (−)
C_{mean}	depth-averaged void fraction (−)
c_{veg}	average grade of vegetation coverage (−)
D'	dimensionless diffusivity (−)
d_{50}	median grain size diameter (mm)
d_c	critical flow depth (m)
D_H	hydraulic diameter (m)
F	bubble count rate (1/s)
f_e	equivalent Darcy-Weisbach friction factor (−)
F_{max}	maximum bubble count rate in a cross-section (1/s)
g	gravitational acceleration (m/s²)

h	step height (m)
H	total head (m)
H_{res}	residual energy (m)
h_u	upstream water level relative to the invert of the broad-crested weir (m)
h_{veg}	average vegetation height (m)
K'	dimensionless integration constant (−)
k_s	equivalent sand roughness height (m)
N	power law exponent (−)
q_w	discharge per unit width (m^2/s)
Re	Reynolds number (−)
S_f	friction slope (−)
u_w	mean flow velocity (m/s)
V	time-averaged interfacial velocity (m/s)
V_{90}	characteristic interfacial velocity where $C = 0.9$ (m/s)
V_c	critical flow velocity (m/s)
x	longitudinal distance along the chute (m)
y	elevation normal to the chute invert (m)
Y_{90}	characteristic flow depth where $C = 0.9$ (m)
Δx	longitudinal separation between probe tips (m)
Δz	transverse separation between probe tips (m)
θ	chute slope (°)
ρ_w	density of water (kg/m^3)
τ	shear stress (N/m^2)
υ	kinematic viscosity of water (m^2/s)

Acknowledgments
The authors thank the technical staff (Manfred Kriegel, Kristian Brodersen, Christian Vogelgesang, and Julian Dreßen) and student assistant Laura Holle for their help with the model tests. The last author thanks Rob Jenkins (WRL, UNSW Sydney) for the manufacturing of the conductivity probes and IWW, RWTH Aachen University for hosting his research visit. The financial support of the project EcoDike (projectno.: 03F0757A) of the German Ministry of Education and Research (BMBF) is acknowledged. The experimental data of the present study are publicly accessible at a data repository (https://doi.org/10.6084/m9.figshare.11787219.v1).

References

Abrahams, A. D., Parsons, A. J., & Wainwright, J. (1994). Resistance to overland flow on semiarid grassland and shrubland hillslopes, Walnut Gulch, southern Arizona. *Journal of Hydrology*, *156*(1-4), 431–446. https://doi.org/10.1016/0022-1694(94)90088-4

Anderson, A. G. (1965). Influence of channel roughness on the aeration of high-velocity, open-channel flow. In *Proceedings of the eleventh Congress of the International Association for Hydraulic Research* (Vol. 1, p. 1–37). Leningrad, Russia: International Association for Hydraulic Research (IAHR).

Barbier, E. B., Hacker, S. D., Kennedy, C., Koch, E. W., Stier, A. C., & Silliman, B. R. (2011). The value of estuarine and coastal ecosystem services. *Ecological Monographs*, *81*(2), 169–193. https://doi.org/10.1890/10-1510.1

Bathurst, J. C. (1988). Velocity profile in high gradient, boulder-bed channels. In *Proceedings of International Conference on Fluvial Hydraulics* (pp. 29–34). Budapest, Hungary: Research Centre for Water Resources Development.

Best, J. (2002). An experimental study of turbulent flow over a low-angle dune. *Journal of Geophysical Research*, *107*(C9), 3135. https://doi.org/10.1029/2000JC000294

Cain, P., & Wood, I. R. (1981). Measurements of self-aerated flow on a spillway. *Journal of the Hydraulics Division*, *107*(11), 1425–1444.

Cantré, S., Olschewski, J., & Saathoff, F. (2017). Full-scale flume experiments to analyze the surface erosion resistance of dike embankments made of dredged materials. *Journal of Waterway, Port, Coastal, and Ocean Engineering*, *143*, 04017001. https://doi.org/10.1061/(ASCE)WW.1943-5460.0000375

Cartellier, A. (1990). Optical probes for local void fraction measurements: Characterization of performance. *Review of Scientific Instruments*, *61*(2), 874–886. https://doi.org/10.1063/1.1141457

Castle, M. E. (1976). A simple disc instrument for estimating herbage yield. *Grass and Forage Science*, *31*(1), 37–40. https://doi.org/10.1111/j.1365-2494.1976.tb01113.x

Chanson, H. (1994). Drag reduction in open channel flow by aeration and suspended load. *Journal of Hydraulic Research*, *32*(1), 87–101. https://doi.org/10.1080/00221689409498791

Chanson, H. (2002a). Air-water flow measurements with intrusive, phase-detection probes: Can we improve their interpretation? *Journal of Hydraulic Engineering*, *128*(3), 252–255. https://doi.org/10.1061/(asce)0733-9429(2002)128:3(252)

Chanson, H. (2002b). *The hydraulics of stepped chutes and spillways*. Lisse, The Netherlands: Balkema.

Chanson, H. (2004). *Environmental hydraulics of open channel flows*. Amsterdam, Boston: Elsevier Butterworth Heinemann.

Chanson, H., & Toombes, L. (2002). Air–water flows down stepped chutes: Turbulence and flow structure observations. *International Journal of Multiphase Flow*, *28*(11), 1737–1761. https://doi.org/10.1016/S0301-9322(02)00089-7

Chapman, J. A., Wilson, B. N., & Gulliver, J. S. (2015). Drag force parameters of rigid and flexible vegetal elements. *Water Resources Research*, *51*, 3292–3302. https://doi.org/10.1002/2014WR015436

CIRIA (2013). *The International Levee Handbook. CIRIA: C731*. London, UK: Construction Industry Research and Information Association (CIRIA).

de Vriend, H. J., van Koningsveld, M., Aarninkhof, S. G. J., de Vries, M. B., & Baptist, M. J. (2015). Sustainable hydraulic engineering through building with nature. *Journal of Hydro-Environment Research*, *9*(2), 159–171. https://doi.org/10.1016/j.jher.2014.06.004

Dean, R. G., Rosati, J. D., Walton, T. L., & Edge, B. L. (2010). Erosional equivalences of levees: Steady and intermittent wave overtopping. *Ocean Engineering*, *37*(1), 104–113. https://doi.org/10.1016/j.oceaneng.2009.07.016

EAK (2002). Empfehlungen für Küstenschutzwerke: Korrigierte Ausgabe 2007. In Kuratorium für Forschung im Küsteningenieurwesen (Ed.), *Die Küste* (Vol. 65). Karlsruhe, Germany: Bundesanstalt für Wasserbau (BAW).

EurOtop (2018). *Manual on wave overtopping of sea defences and related structures. An overtopping manual largely based on European research, but for worldwide application*. J. W. Van der Meer, N. W. H. Allsop, T. Bruce, J. de Rouck, A. Kortenhaus, T. Pullen, H. Schüttrumpf, P. Troch, & B. Zanuttigh (Eds.). www.overtopping-manual.com

Felder, S. (2013). Air-water flow properties on stepped spillways for embankment dams: Aeration, energy dissipation and turbulence on uniform, non-uniform and pooled stepped chutes (Doctoral dissertation). University of Queensland, Brisbane, Australia. Retrieved from https://espace.library.uq.edu.au/view/UQ:301329

Felder, S. (2018). StefanFelder/Air-water-flow-data-analysis-software-for-double-tip-phase-detection-intrusive-probes: Zenodo.

Felder, S., & Chanson, H. (2013). Aeration, flow instabilities, and residual energy on pooled stepped spillways of embankment dams. *Journal of Irrigation and Drainage Engineering*, *139*(10), 880–887. https://doi.org/10.1061/(ASCE)IR.1943-4774.0000627

Felder, S., & Chanson, H. (2015a). Aeration and air–water mass transfer on stepped chutes with embankment dam slopes. *Environmental Fluid Mechanics*, *15*(4), 695–710. https://doi.org/10.1007/s10652-014-9376-x

Felder, S., & Chanson, H. (2015b). Phase-detection probe measurements in high-velocity free-surface flows including a discussion of key sampling parameters. *Experimental Thermal and Fluid Science*, *61*, 66–78. https://doi.org/10.1016/j.expthermflusci.2014.10.009

Felder, S., & Chanson, H. (2015c). Simple design criterion for residual energy on embankment dam stepped spillways. *Journal of Hydraulic Engineering*, *142*, 04015062. https://doi.org/10.1061/(ASCE)HY.1943-7900.0001107

Felder, S., & Chanson, H. (2016). An experimental study of air-water flows in hydraulic jumps with channel bed roughness: WRL Research Report, WRL 259. Retrieved from http://handle.unsw.edu.au/1959.4/unsworks_40454

Felder, S., Hohermuth, B., & Boes, R. M. (2019). High-velocity air-water flows downstream of sluice gates including selection of optimum phase-detection probe. *International Journal of Multiphase Flow*, *116*, 203–220. https://doi.org/10.1016/j.ijmultiphaseflow.2019.04.015

Felder, S., & Pfister, M. (2017). Comparative analyses of phase-detective intrusive probes in high-velocity air-water flows. *International Journal of Multiphase Flow*, *90*, 88–101. https://doi.org/10.1016/j.ijmultiphaseflow.2016.12.009

Felder, S., & Severi, A. (2016). Entrapped air in high-velocity free-surface flows on a flat-sloped spillway. In *Proc. of 20th Australasian Fluid Mechanics Conference*. Retrieved from http://handle.unsw.edu.au/1959.4/unsworks_42463

Ferro, V., & Baiamonte, G. (1994). Flow velocity profiles in gravel-bed rivers. *Journal of Hydraulic Engineering*, *120*(1), 60–80. https://doi.org/10.1061/(ASCE)0733-9429(1994)120:1(60)

Gambi, M. C., Nowell, A. R. M., & Jumars, P. A. (1990). Flume observations on flow dynamics in *Zostera marina* (eelgrass) beds. *Marine Ecology Progress Series*, *61*, 159–169. https://doi.org/10.3354/meps061159

Gehlker, H. (1977). Eine Hilfstafel zur Schätzung von Deckungsgrad und Artmächtigkeit. *Mitteilungen der Florist.-Soziol. Arbeitsgemeinschaft NF*, *19*(20), 427–429.

Graunke, A., & Wrage-Mönnig, N. (2018). Grüne Seedeiche für den Küstenschutz. In Institut für Pflanzenbau und Pflanzenzüchtung der Christian-Albrechts-Universität zu Kiel (Ed.), *Leistungen von Gras und Klee-Gras auf Acker und Grünland* (pp. 95–99). Retrieved from https://www.lfl.bayern.de/mam/cms07/ipz/dateien/aggf_2018_graunke_wrage_moennig.pdf

Gutiérrez, J. L., Jones, C. G., Byers, J. E., Arkema, K. K., Berkenbusch, K., Commito, J. A., et al. (2011). Physical ecosystem engineers and the functioning of estuaries and coasts. In E. Wolanski, & D. S. McLusky (Eds.), *Treatise on Estuarine and Coastal Science* (Vol. 7, pp. 53–81). Amsterdam, The Netherlands: Elsevier/Academic Press. https://doi.org/10.1016/B978-0-12-374711-2.00705-1

Henderson, F. M. (1966). *Open channel flow*. Upper Saddle River NJ: Prentice Hall.

Hewlett, H. W. M., Boorman, L. A., & Bramley, L. A. (1987). *Design of reinforced grass waterways*, *CIRIA report* (Vol. 116). London, UK: Construction Industry Research and Information Association.

Hughes, S. A. (2011). Adaptation of the levee erosional equivalence method for the hurricane storm damage risk reduction system (HSDRRS): ERDC/CHL TR-11-3. Retrieved from U.S. Army Corps of Engineers, Coastal & Hydraulics Laboratory, Engineer Research and Development Center, Vicksburg, Mississippi website: https://apps.dtic.mil/dtic/tr/fulltext/u2/a543973.pdf

Hunt, S. L., Kadavy, K. C., & Hanson, G. J. (2014). Simplistic design methods for moderate-sloped stepped chutes. *Journal of Hydraulic Engineering*, *140*, 04014062. https://doi.org/10.1061/(ASCE)HY.1943-7900.0000938

Järvelä, J. (2002). Flow resistance of flexible and stiff vegetation: a flume study with natural plants. *Journal of Hydrology*, *269*(1-2), 44–54. https://doi.org/10.1016/S0022-1694(02)00193-2

Kothyari, U. C., Hayashi, K., & Hashimoto, H. (2009). Drag coefficient of unsubmerged rigid vegetation stems in open channel flows. *Journal of Hydraulic Research*, *47*(6), 691–699. https://doi.org/10.3826/jhr.2009.3283

Le, H. T., Verhagen, H. J., & Vrijling, J. K. (2017). Damage to grass dikes due to wave overtopping. *Natural Hazards*, *86*(2), 849–875. https://doi.org/10.1007/s11069-016-2721-2

Lightbody, A. F., & Nepf, H. M. (2006). Prediction of velocity profiles and longitudinal dispersion in salt marsh vegetation. *Limnology and Oceanography*, *51*(1), 218–228. https://doi.org/10.4319/lo.2006.51.1.0218

Morris, R. L., Konlechner, T. M., Ghisalberti, M., & Swearer, S. E. (2018). From grey to green: Efficacy of eco-engineering solutions for nature-based coastal defence. *Global Change Biology*, *24*(5), 1827–1842. https://doi.org/10.1111/gcb.14063

Mossa, M., Ben Meftah, M., de Serio, F., & Nepf, H. M. (2017). How vegetation in flows modifies the turbulent mixing and spreading of jets. *Scientific Reports*, *7*(1), 6587. https://doi.org/10.1038/s41598-017-05881-1

Murphy, E., Ghisalberti, M., & Nepf, H. (2007). Model and laboratory study of dispersion in flows with submerged vegetation. *Water Resources Research*, *43*, 67. https://doi.org/10.1029/2006WR005229

Narayan, S., Beck, M. W., Reguero, B. G., Losada, I. J., van Wesenbeeck, B., Pontee, N., et al. (2016). The effectiveness, costs and coastal protection benefits of natural and nature-based defences. *PloS One*, *11*, e0154735. https://doi.org/10.1371/journal.pone.0154735

Nepf, H. M. (2012a). Flow and transport in regions with aquatic vegetation. *Annual Review of Fluid Mechanics*, *44*(1), 123–142. https://doi.org/10.1146/annurev-fluid-120710-101048

Nepf, H. M. (2012b). Hydrodynamics of vegetated channels. *Journal of Hydraulic Research*, *50*(3), 262–279. https://doi.org/10.1080/00221686.2012.696559

Pagliara, S., Carnacina, I., & Roshni, T. (2010). Self-aeration and friction over rock chutes in uniform flow conditions. *Journal of Hydraulic Engineering*, *136*(11), 959–964. https://doi.org/10.1061/(ASCE)HY.1943-7900.0000270

Pan, C., Ma, L., Wainwright, J., & Shangguan, Z. (2016). Overland flow resistances on varying slope gradients and partitioning on grassed slopes under simulated rainfall. *Water Resources Research*, *52*, 2490–2512. https://doi.org/10.1002/2015WR018035

Press, H., & Schröder, R. (1966). *Hydromechanik im Wasserbau*. Berlin, München: Ernst.

Scheres, B., Graunke, A., Wrage-Mönnig, N., & Schüttrumpf, H. (2018). Full-scale model tests on the erosion resistance of ecologically valuable sea dike vegetation. In *Proceedings of the 9th Chinese-German Joint Symposium on Hydraulic and Ocean Engineering* (pp. 329–337).

Scholl, B. N. (2016). Bulking coefficients of aerated flow during wave overtopping simulation on protected land-side slopes (Doctoral dissertation). Colorado State University, Fort Collins, Colorado. Retrieved from https://mountainscholar.org/handle/10217/176666

Schoonees, T., Gijón Mancheño, A., Scheres, B., Bouma, T. J., Silva, R., Schlurmann, T., & Schüttrumpf, H. (2019). Hard structures for coastal protection, towards greener designs. *Estuaries and Coasts*, *42*(7), 1709–1729. https://doi.org/10.1007/s12237-019-00551-z

Schüttrumpf, H., & Oumeraci, H. (2005). Layer thicknesses and velocities of wave overtopping flow at seadikes. *Coastal Engineering*, *52*(6), 473–495. https://doi.org/10.1016/j.coastaleng.2005.02.002

Severi, A. (2018). Aeration performance and flow resistance in high-velocity flows over moderately sloped spillways with micro-rough bed (Doctoral dissertation). UNSW Sydney, Sydney, Australia. Retrieved from http://unsworks.unsw.edu.au/fapi/datastream/unsworks:54742/SOURCE02?view

Straub, L. G., & Anderson, A. G. (1960). Self-aerated flow in open channels. *Journal of the Hydraulics Division*, 456–486.

Sutton-Grier, A. E., Gittman, R. K., Arkema, K. K., Bennett, R. O., Benoit, J., Blitch, S., et al. (2018). Investing in natural and nature-based infrastructure: Building better along our coasts. *Sustainability*, *10*, 523. https://doi.org/10.3390/su10020523

Termini, D. (2015). Flexible vegetation behaviour and effects on flow conveyance: Experimental observations. *International Journal of River Basin Management*, *13*(4), 401–411. https://doi.org/10.1080/15715124.2015.1012519

Toombes, L., & Chanson, H. (2007). Surface waves and roughness in self-aerated supercritical flow. *Environmental Fluid Mechanics*, *7*(3), 259–270. https://doi.org/10.1007/s10652-007-9022-y

Velasco, D., Bateman, A., Redondo, J. M., & DeMedina, V. (2003). An open channel flow experimental and theoretical study of resistance and turbulent characterization over flexible vegetated linings. *Flow, Turbulence and Combustion (formerly Applied Scientific Research)*, *70*(1-4), 69–88. https://doi.org/10.1023/B:APPL.0000004932.81261.40

Wood, I. R. (1983). Uniform region of self-aerated flow. *Journal of Hydraulic Engineering*, *109*(3), 447–461. https://doi.org/10.1061/(ASCE)0733-9429(1983)109:3(447)

Wüthrich, D., & Chanson, H. (2014). Hydraulics, air entrainment, and energy dissipation on a gabion stepped weir. *Journal of Hydraulic Engineering*, *140*, 4014046. https://doi.org/10.1061/(ASCE)HY.1943-7900.0000919

Yang, J. Q., Kerger, F., & Nepf, H. M. (2015). Estimation of the bed shear stress in vegetated and bare channels with smooth beds. *Water Resources Research*, *51*, 3647–3663. https://doi.org/10.1002/2014WR016042

Yang, W., & Choi, S.-U. (2010). A two-layer approach for depth-limited open-channel flows with submerged vegetation. *Journal of Hydraulic Research*, *48*(4), 466–475. https://doi.org/10.1080/00221686.2010.491649

Zhang, G., & Chanson, H. (2017). Self-aeration in the rapidly- and gradually-varying flow regions of steep smooth and stepped spillways. *Environmental Fluid Mechanics*, *17*(1), 27–46. https://doi.org/10.1007/s10652-015-9442-z

Zhao, C., Gao, J., Huang, Y., Wang, G., & Zhang, M. (2016). Effects of vegetation stems on hydraulics of overland flow under varying water discharges. *Land Degradation & Development*, *27*(3), 748–757. https://doi.org/10.1002/ldr.2423